Influence of rotation frequency and rotation diameter on mechanical properties and microstructure of weld metal produced by MCAW-RE

Guilherme M. S. Silveira, Walker A. S. Filho, Jeferson F. M. Costa, Matheus C. Mendes, Luís Felipe G. Souza & Jorge C. F. Jorge

The International Journal of Advanced Manufacturing Technology

ISSN 0268-3768

Int J Adv Manuf Technol
DOI 10.1007/s00170-020-05961-z

ONLINE FIRST

Springer

The International Journal of Advanced Manufacturing Technology
https://doi.org/10.1007/s00170-020-05961-z

ORIGINAL ARTICLE

Influence of rotation frequency and rotation diameter on mechanical properties and microstructure of weld metal produced by MCAW-RE

Guilherme M. S. Silveira [1] · Walker A. S. Filho [1] · Jeferson F. M. Costa [1] · Matheus C. Mendes [1] · Luís Felipe G. Souza [1] · Jorge C. F. Jorge [1]

Received: 15 May 2020 / Accepted: 17 August 2020

Abstract

The MCAW process with rotating electrode (MCAW-RE) is a variation of the conventional gas metal arc welding process, which a metal-cored wire is submitted to a rotational movement along a pre-established diameter. This process enhances narrow gap welding, since the rotational motion of the electrode allows the electric arc to reach peripheral regions of the groove, preventing lack of fusion on the sidewall. As a result, reduced costs and superior productivity compared with the conventional GMAW process are obtained. The limited literature about this process is focused on the operational characteristics, and works studying the mechanical properties are not available. Thus, this work evaluates the mechanical and microstructural properties of weld metals obtained by the MCAW-RE process in order to allow a decision about its technical feasibility to replace the GMAW process in industry. Initially, beads on plate weld tests were performed with varying rotation frequency and rotation diameter, in order to determine the parameters to be used in welded joints. High-strength steel weld metals were obtained by welding performed in steel plates with dimensions of 500 × 300 × 10 mm. Mechanical tests and metallographic examination were carried out in samples removed transversally to the weld bead. The results showed that the impact toughness of the weld metals can achieve the requirements for several industrial applications. The results showed that the GMAW process with rotating electrode-cored wire has a high potential for replacement of the GMAW in industrial applications.

Keywords MCAW-RE process · Rotating electrode · Mechanical properties · Impact toughness · Microstructure

1 Introduction

Based on the improvement of the thermo-mechanical processing routes and heat treatments, high-strength low-alloy (HSLA) steels have been developed to several applications in oil and gas, shipbuilding, and pipeline industries where frequently thick steel products are used [1, 2]. Since welding is usually applied in manufacturing and repair operations of industrial components [3], the development of new welding processes, aiming for improvement of productivity allied with quality and low costs, has been motivated. In this respect, it is known that GMAW (gas metal arc welding) process is widely used at most diverse applications, due to its characteristics of high deposition rate, versatility, easily adaptable for automation and relatively low cost in comparison with other electric arc processes [4–6]. With the improvement of power sources, the field of application of the process has become even wider [7].

Although there are some developments available in market as laser-arc hybrid welding (LAHW), its applicability is under concern because it requires a sophisticated optimization of process parameters for suitability due to its complexity [2], which can be an issue for operations in situ.

GMAW process with rotating electrode (GMAW-RE) is a variation of the conventional GMAW process, where the continuously fed electrode into a molten pool is submitted to a rotating movement, with pre-established rotation diameter and frequency. The radial projection of the metallic droplets reduces the risk of sidewalls lack of fusion, which historically is a limitation of the GMAW process [8]. It contributes to the feasibility of welding in narrow gap, with significant reduction of deposited weld metal and welding time and preparation of the joint and residual strength levels [9, 10].

✉ Jorge C. F. Jorge
jorgecfjorge@gmail.com; jorge.jorge@cefet-rj.br

[1] Departamento de Engenharia Mecânica, Centro Federal de Educação Tecnológica Celso Suckow da Fonseca (CEFET-RJ), Av. Maracanã, 229, CEP, Rio de Janeiro, RJ 20271-110, Brazil

Published online: 28 August 2020

Table 1 Chemical composition of the materials

Element (wt%)	C	Si	Mn	P	S	Cr	Mo	Ni	Cu	Ti
Base metal	0.17	0.19	1.15	0.013	0.005	0.02	-	0.02	0.026	0.015
Weld metal BOP*	0.12	0.46	1.52	0.010	0.005	0.11	0.31	1.12	0.038	0.025
Weld metal welded joint	0.13	0.48	1.37	0.013	0.008	0.13	0.48	1.61	0.039	0.022
Weld metal—supplier**	0.06	0.58	1.72	0.010	0.013	0.20	0.50	1.84	-	-

* Sampled from bead on plate

** Chemical composition expected for welds obtained with 10% CO_2

A relevant question involves the correct terminology applied to the GMAW process with rotating electrode, because some authors [10–14] have chosen to designate the process as GMAW with rotating arc. In recent review of the terminology of the metal transfer modes of the conventional GMAW process, Kah et al. [12] have established that a rotating metallic transfer occurs for higher energy bands, resulting from a long electrode length or "stick out" (25 to 35 mm) associated with high currents and voltages of the electric arc. In this case, from the conventional GMAW process, rotation occurs only in the electric arc at the wire end and is caused by electromagnetic forces acting on it. Therefore, the designation GMAW with rotating arc for this new process can cause some confusion if it is not specified whether the origin of the rotation is electromagnetic or mechanical, once they refer to processes with different characteristics. Other authors [14, 15] mention the process as GMAW with rotating electrode (GMAW-RE), while Zhang et al. [16] designate it as a GMAW process with rotating wire (GMAW-RW). In these two cases, the difference is subtle, since in general, the wire used in the GMAW process is also the electrode. The exception occurs when there is the addition of an extra wire, which may be cold or hot, but regardless of whether it is one or the other, the extra wire does not figure as an electrode in the process. There are also some works [14, 15] in which it is possible to find mention of the process by its trademark "Spin Arc." Just as it is not uncommon to find in the same text, more than one of these forms presented, which shows that there is a lack of standardization in the designation of the process. In the present work, the designation adopted for the GMAW process with rotating electrode is GMAW-RE or MCAW-RE, for solid and metal cored wires, respectively.

GMAW-RE process introduces a modification over the conventional one that influences the mode of metallic transfer of the wire to the melt pool and the distribution of heat in the joint [9, 10, 13, 17, 18]. The rotational movement accelerates the metallic droplets radially, due to centrifugal force, and this effect depends essentially on the diameter and speed of rotation [11]. According to Prasad et al. [10], this process promotes an increase in productivity and quality in welding made with both solid and tubular wires.

Although there are some studies about operational characteristics of the process [9, 11, 15, 19, 21], the literature involving mechanical properties of welded joints is still very limited and inconclusive [22–24], and more experimental evidences are necessary to confirm the potential of this process.

This work studies the mechanical and microstructural properties of welded joints obtained by GMAW with rotating electrode process using metal-cored wire (MCAW-RE).

Table 2 Welding parameters used for deposition of BOP deposits

BOP number	Rotation diameter (mm)	Rotation frequency (rpm)
1	3	1500
2	3	3000
3	3	5000
4	6	1500
5	6	3000
6	6	5000
7	8	1500
8	8	3000
9	8	5000

2 Materials and methods

2.1 Materials and welding

ASTM A 516 Grade 70 steel plates with 500 × 300 × 10 mm were used as base metal. As welding consumable, a 1.2-mm

Table 3 Welding parameters

Current (A)	Voltage (V)	Welding speed (mm/s)	Wire feed speed (mm/s)	Heat input (kJ/mm)	Number of passes
248	28	3.14	145	2.0	2

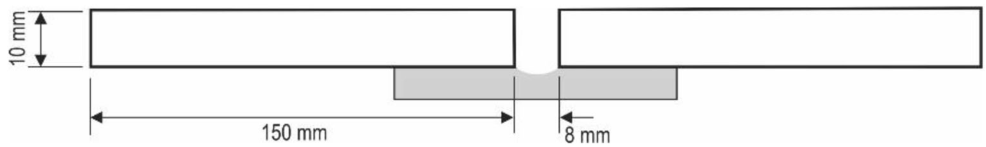

Fig. 1 Weld joint geometry

diameter AWS A 5.28 E110C-K4H4 [25] metal-cored wire was used as filler metal.

Table 1 shows the chemical composition of the materials obtained by optical emission spectroscopy.

Initially, bead on plate (BOP) tests were performed to evaluate the influence of the rotation frequency and rotation diameter on the characteristics of the weld beads. Table 2 shows the conditions used in this experiment.

Welding was carried out in flat position using electrical parameters obtained from preliminary tests, the average current being 240A, the average voltage 28 V and the average welding speed 4.0 mm/s.

After BOP tests, a welded joint was obtained using the joint geometry illustrated in Fig. 1. Welding was performed in flat position, preheat of 100 °C, and interlayer temperature was maintained at 150 °C. In addition, a frequency of 1500 rpm and a diameter of 3 mm were employed based on the results obtained in BOP tests. The welding parameters (Table 3) and joint geometry were adjusted after preliminary tests to obtain defect free welded joints.

Ar-10%CO_2 with a flow rate of 20 L/min were applied as shielding gas, and the welding parameters were obtained from a portable welding parameter monitoring system, with an acquisition rate of 5 kHz.

After welding, the welded joint was submitted to a nondestructive examination, by magnetic particle testing (MPT) and ultrasonic testing (UT). No defects or flaws had been detected during inspection.

2.2 Mechanical tests

Vickers microhardness tests with 500-gf load were performed within the weld metals and points located at the positions showed in Fig. 2 to elucidate the changes on this property due to the rotation of the electrode

From welded joints, specimens were sampled at the mid-thickness for impact Charpy-V and microhardness tests.

Charpy-V impact tests at − 40, − 20, 0, and 20 °C temperatures were performed on reduced test pieces (5 × 10 × 55 mm) removed transversally to the weld bead. The notch was positioned in the thickness section at position corresponding to the weld metal centerline as shown in Fig. 3.

Vickers microhardness tests with 500-gf load were performed at points located within the weld metals as depicted in Fig. 4.

2.3 Metallographic examination

Initially, transverse sections were removed from BOP samples, and a detailed examination by optical microscopy (OM) was carried out to evaluate the influence of the frequency and diameter on geometrical characteristics of

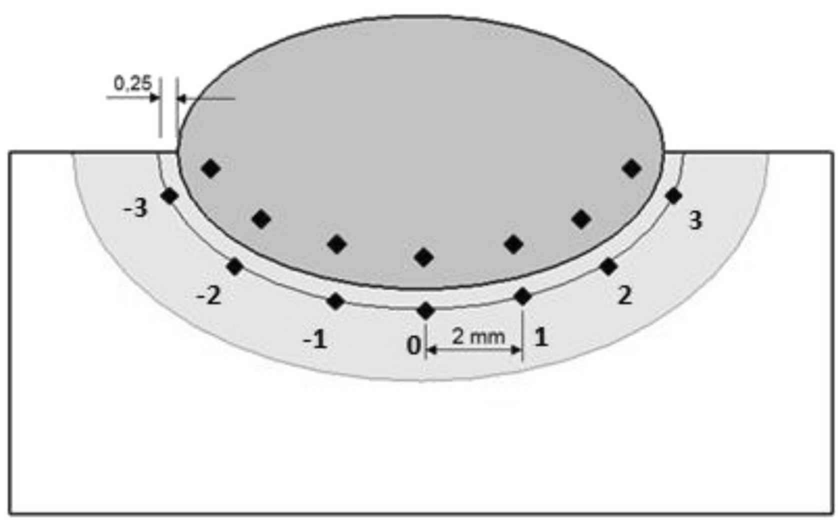

Fig. 2 Position of microhardness measurements in BOP samples

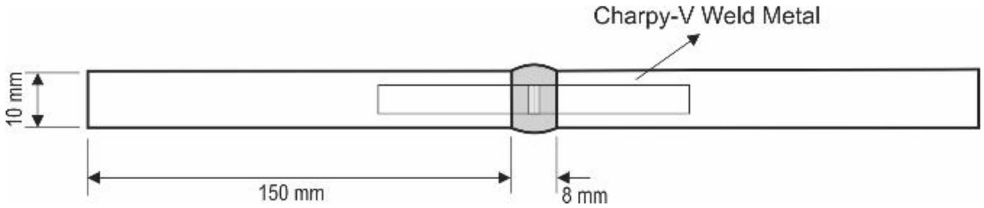

Fig. 3 Position of Charpy-V impact test specimen

the weld deposits. Aspects as penetration, width and dilution were measured directly on the OM screen by using the Stream Essentials image analysis software. The global dilution was determined in the transverse cross section by the ratio between substrate diluted area and total diluted area with the aid of the AutoCAD software. Both areas were measured, and the ratio between them was calculated.

Scanning electron microscopy (SEM) and electron backscattering diffraction (EBSD) techniques were also used to clarify the microstructure of some selected samples, in order to define the welding parameters for later use in the square butt joint.

From welded joint, transverse sections were prepared, and a detailed examination by OM, SEM, and EBSD in samples removed from regions related to the positioning of the Charpy-V notch was carried out to clarify the main microstructural constituents, microphases, and inclusions.

Quantitative analysis was done by a point-counting technique using a 10 × 10 grid on the optical microscope screen, in order to identify the following microstructural constituents: primary ferrite (PF), ferrite with second phase (FS), acicular ferrite (AF), and martensite (M). At least 1000 points were counted for each condition with a nominal magnification of × 1000.

Quantitative measurements of microphases and inclusions were performed by selecting ten different fields which were observed by SEM with a nominal magnification of × 2500 for microphases and × 1500 for inclusions. A binarization of the images collected was performed using ImageJ software, followed by calculation of area fraction of the microphases.

Semi-quantitative analysis of some elements was assessed by energy-dispersive spectroscopy (EDS), to characterize the composition of inclusions, matrix, and microphases.

The EBSD maps were collected with SEM operating at 20 kV and step size of 0.3 μm. A post-processing (reconstructed map) of the EBSD data was conducted by using the HKL Channel 5 software package. Matrix grain orientation was interpreted by the inverse pole figure (IPF) in Z direction (transverse direction, perpendicular to the screen). High-angle grain boundaries (HAGBs, misorientation > 15°) [26] were distinguished by the scalar misorientation between the adjacent pixels. Effective grain size (EGS) of the grains with HAGBs was measured from the grain boundary maps with the line-intercept method. Grain average misorientation (GAM) with a 1.0-degree threshold was used to categorize grains as recrystallized, partially recrystallized, or un-recrystallized. Grains with an internal GAM exceeding the threshold are categorized as un-recrystallized. Grains are classified as partially recrystallized when the GAM is lower than the threshold, but the misorientation between sub-grains exceeds the threshold. Finally, recrystallized grain has a GAM and sub-grain misorientation lower than the thresholds or has no sub-grains [27].

The samples were prepared using the conventional procedure of grinding and polishing with diamond paste of 6, 3, and 1 μm. For EBSD, automatic polishing with 0.06 μm colloidal silica suspension was also used. Unetched samples were used

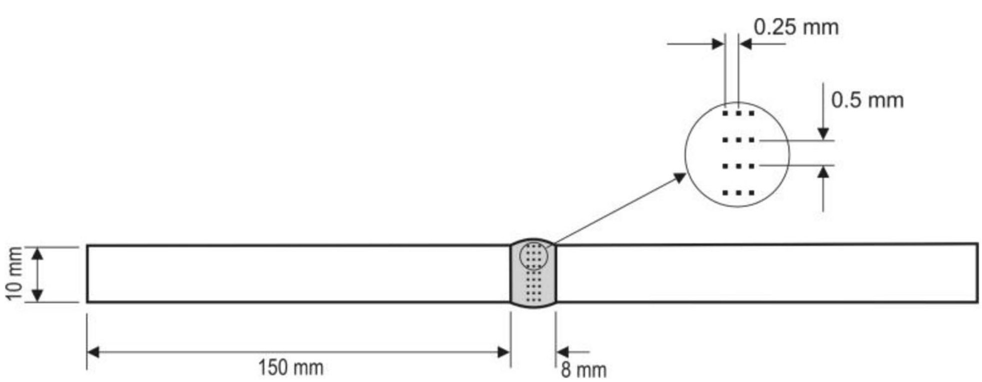

Fig. 4 Position of microhardness measurements in welded joint

Table 4 Geometrical measurements of the BOP samples

Rotation diameter (mm)	Rotation frequency (rpm)	Penetration (mm)	Width (mm)	Dilution (%)	Average extension of the HAZ (mm)
3	1500	2.83	13.49	39	1.76
	3000	2.79	13.63	43	1.83
	5000	1.47	14.79	36	2.22
6	1500	2.69	13.69	40	1.88
	3000	1.58	14.38	40	2.24
	5000	0.75	15.55	27	2.61
8	1500	1.83	14.32	38	2.11
	3000	1.27	14.54	33	2.50

for EBSD and identification of inclusions, while microstructural constituents and microphases were observed after etching with 2% nital.

3 Results

3.1 BOP experiments

The macrographs obtained from BOP samples are showed in Fig. 5. In general, the penetration decreases, and the weld beads become wider by increasing rotation diameter and frequency (Table 4). Also, defects are observed in weld deposits performed with the higher frequency. The welding using 5000 rpm and 8 mm did not provide an appropriate weld bead because the electrical arc was instable and erratic. Moreover, the extension of the heat-affected zone (HAZ) is also increased with increasing rotation diameter and frequency. Thus, it indicates that higher rotation diameters and frequencies are not suggested to be used.

Figure 6 shows the average hardness of the weld metals obtained along the fusion line. While the hardness is more homogeneous for 3mm and a slight increase is observed for 5,000 rpm, significant changes on this property can be observed when frequency is increased for a rotation diameter of 6 mm.

Based on these evidences, additional investigation by the OM, SEM, and EBSD techniques were conducted for samples obtained with 3-mm diameter, due to their more homogeneous and representative behavior.

Figures 7 and 8 show the OM and SEM images obtained at the point where the higher hardness values were obtained. It is seen that OM analysis is not able to clarify the microstructural constituents, even using a high magnification (× 1000). The SEM images (Fig. 8) show that the refined microstructure is composed by acicular ferrite (AF), primary ferrite (PF), and ferrite with second phase. The presence of martensitic areas (M) on the weld metal obtained with the higher frequency is also noted (Fig. 8c). It is worthy of note the contribution of the titanium to the microstructure refinement which is characterized by the

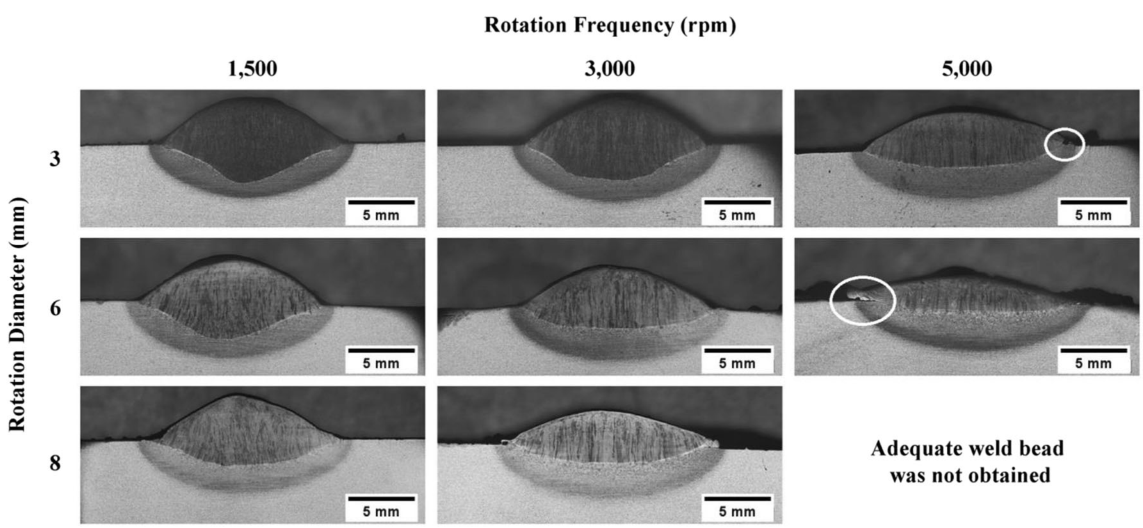

Fig. 5 Macrographs of the BOP samples after etching with 2% nital. Welding defects are indicated by the circles.

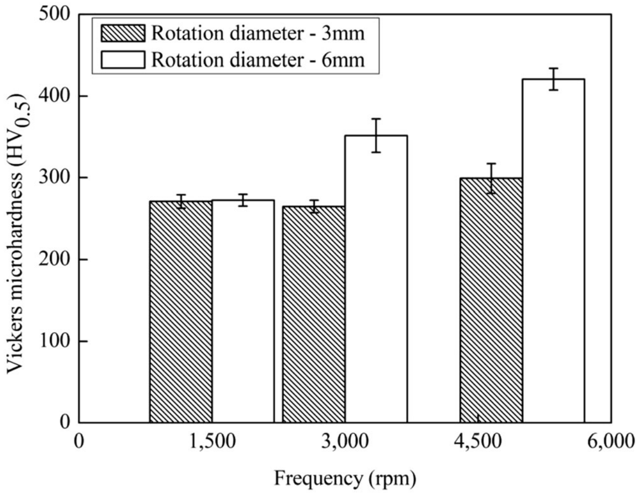

Fig. 6 Behavior of microhardness results for BOP samples

presence of inclusions acting as preferential sites for nucleation of acicular ferrite (Fig. 9).

As the refined microstructures are very similar, EBSD technique was applied as a complementary tool to detail some useful characteristics, as showed in Fig. 10 and Table 5. Although the effective grain size is the same for all samples, significant changes are showed in the HAGB frequency for 1500 rpm. In addition, the GAM maps evidence that, for 5000 rpm, the most grains are deformed grains with high-strain energy levels. Matrix components were classified into recrystallized (blue), sub-structured (yellow), and deformed grains (red) using GAM evaluation to distinguish the local strain energy difference. The recrystallized and deformed grains have the lowest and highest local strain energy, respectively [28].

EGS effective grain size, *HAGB* high-angle grain boundary

3.2 Welded joint

Figure 11 shows the macrograph of the welded joint, where the effect of the multipass welding and the absence of defects can be noted.

Figure 12 shows the general aspect of the microstructure of the weld metal observed by OM, where the presence of acicular ferrite (~ 11%), primary ferrite (~ 17%), and predominance of ferrite with second phase (~ 72%) is observed. The presence of inclusions was investigated by SEM (Fig. 13), and the results revealed a mean size of 0.71 μm.

SEM analysis showed that MA constituents are the main microphases occurring in weld metal (Fig. 14). Interestingly, the results are very similar for columnar and reheated regions with an average volume fraction of microphases of 18% for each region. It is confirmed by EBSD analysis, as showed in Figs. 15 and 16.

Figure 17 shows the microhardness behavior of the weld metals, where differently from the expected behavior, the effect of reheating did not promote a continuous decrease from top surface to the root.

Figure 18 shows the impact toughness for different temperatures, where it is worth noting the average results superior to 27 J for low temperatures, even using sub-size specimens (5 × 10 mm)

4 Discussion

4.1 Mechanical and microstructural properties of the BOP samples

It was previously said that there are many other authors studying the effect of parameters on the characteristics of weld beads produced by the GMAW process with rotating electrode [8, 10, 14, 20, 22, 29–31]. In general, they show that the penetration decreases with increasing the frequency [14, 29]. However, the beads deposited by rotating arc process are flat and semi-circular instead of the finger-type penetration, where the penetration is deep and narrow at the center of the bead [8, 22, 29, 30], so the fusion of the side walls are promoted and the lack of fusion is avoided. Bai et al. [20] showed that the temperature at the centerline of weld metal is reduced by increasing the diameter. Although there are no systematic works involving the influence of frequency and diameter, the original values were based on these works available in literature [8, 20, 22, 29, 30].

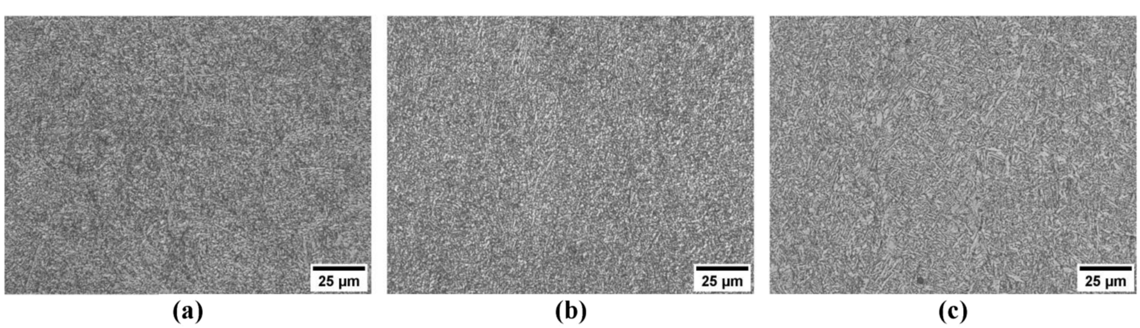

Fig. 7 OM images of the BOP samples for 3-mm diameter after etching with 2% nital. **a** 1500 rpm, **b** 3000 rpm, and **c** 5000 rpm

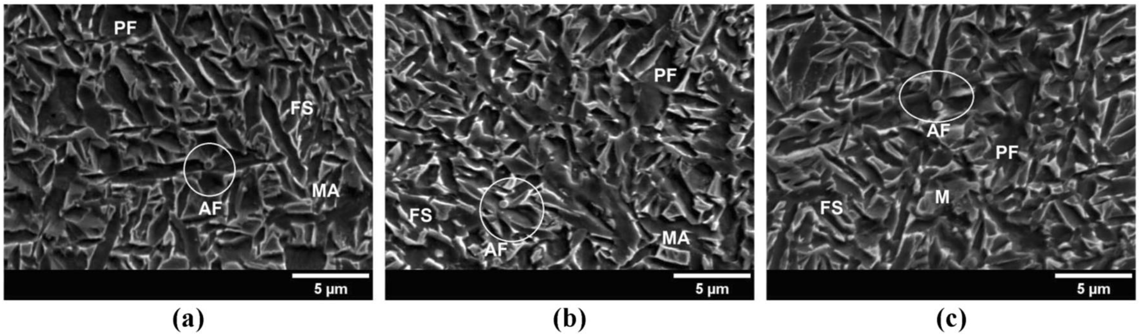

Fig. 8 SEM images of the BOP samples for 3-mm diameter after etching with 2% nital. **a** 1500 rpm, **b** 3000 rpm, and **c** 5000 rpm. Inclusion nucleant of acicular ferrite are circled

The microstructural characterization performed in this work involved the use of OM, SEM, and EBSD as complementary techniques due to the very refined microstructures. Indeed, it is important to emphasize that the OM, even using a higher magnification than that recommended by the International Institute of Welding [32], was unable to clarify the microstructure and to allow a selection of the more appropriate parameters to weld the square butt joint. However, when observing the analysis provided by the EBSD technique, it is clear the advantages of using 1500 rpm, because this sample presents significant and improved differences in comparison with the other samples, mainly the higher frequency of HAGB (> 45°), which is related to a higher amount of acicular ferrite [33–35]. On the contrary, the higher frequency shows results usually associated with the presence of martensite, which is in agreement with the higher hardness obtained.

This behavior results from the particular thermal cycle of the process, since the peak temperature on weld metal center and on HAZ becomes smaller and greater, respectively, as compared with conventional GMAW [10]. In addition, the results of this work show that, as the rotation frequency increases, this effect intensifies, once the hardness and the extension of HAZ are also increased. EBSD analysis corroborate this proposition, where the large percentage of deformed grains (red) in the 5000-rpm sample indicates the formation of martensitic areas, in contrast to the 1500-rpm sample.

In general, the best results were obtained for 3-mm rotation diameter, except when comparison is made with the weld beads obtained with 6-mm rotation diameter using 1500 rpm. However, considering the necessity to improve the productivity and reduction of costs, it does not seem reasonable to use a higher rotation diameter, because it means to deposit much more material (double) as consequence of the superior root opening to be applied in joint geometry.

Besides, welding defects and operational issues might be caused by using of high parameters. By raising the rotation frequency values, an increase of the shielding gas flow is needed in order to avoid porosity, once the intensification of rotation movement induces a turbulence and dispersion of the gas flow. As result, total welding costs also increases due to the greater volume of gas necessary. Regarding high rotation diameters, too large angular amplitude might promote the climb of the electric arc on the bevel walls, resulting in lack of fusion on the sidewalls, especially in root pass [36]. The combination of high parameters also creates instability in the formation of the weld pool, caused by the intense radial projection of the molten metal droplets, which leads to a high rate of spatter during welding.

Thus, it strongly implies that higher frequencies and diameters are not recommended for welding of square butt joints.

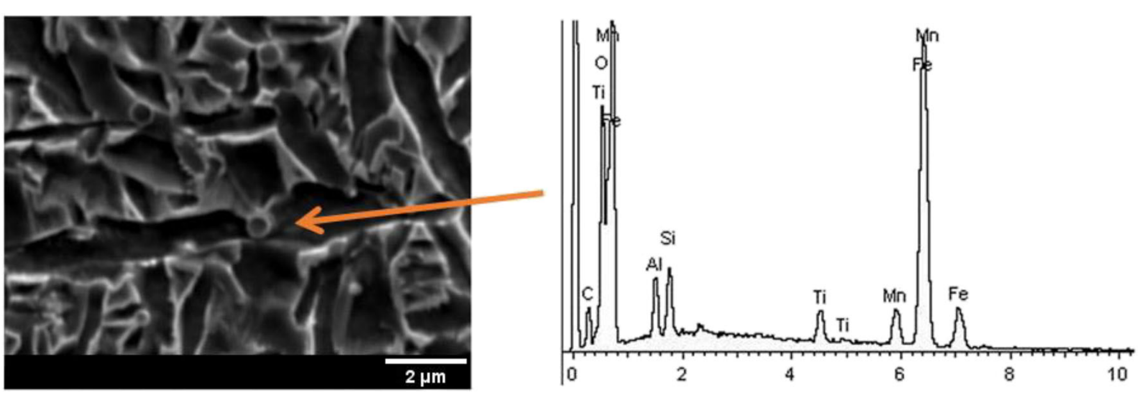

Fig. 9 Evidence of inclusion containing Ti on the nucleation of acicular ferrite (SEM). Etching: 2% nital

Table 5 EBSD grain boundary, grain size, and GAM analyses of the BOP samples

Sample	1500 rpm	3000 rpm	5000 rpm
EGS (μm)	1.5	1.5	1.5
HAGB frequency (> 15°, %)	55	45	40
HAGB frequency (> 45°, %)	47	36	33
Recrystallized grain frequency (%)	20	12	9
Substructured grain frequency (%)	40	41	15
Deformed grain frequency (%)	41	48	76

The results obtained in this work and the discussion showed that the association of a 1500-rpm rotation frequency and 3-mm rotation diameter presented the best performance and therefore is the proper combination to weld.

4.2 Mechanical and microstructural properties of the welded joint

The control of weld metal microstructure as well as raising the welding productivity are critical factors for the development of weld metal of high-strength steel, to secure satisfactory mechanical properties and to reduce production costs [37].

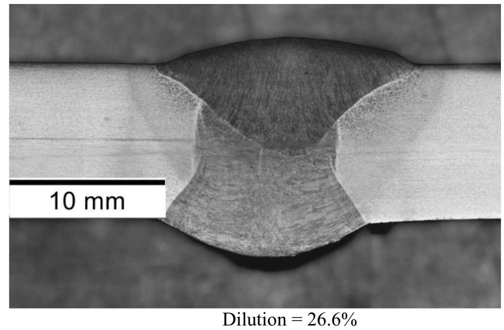

Fig. 11 Macrograph of welded joint after etching with 2% nital (OM). Dilution, 26.6%

Although presenting an advantage of lower volume of deposited weld metal, the application of square groove geometry can promote deleterious effects on the mechanical properties due to the higher dilution with base metal [1, 3, 38–40]. It is seen in Fig. 11, where a superior dilution was found (26.6%) in comparison with that provided by GMAW process (19.3%) observed in previous work using solid wire [41], which can affect the phase transformation kinetics during weld-induced thermal cycles, as well as the resultant microstructures [39]. The chemical composition of the weld metal confirms the effect of dilution, where an increase in carbon content and

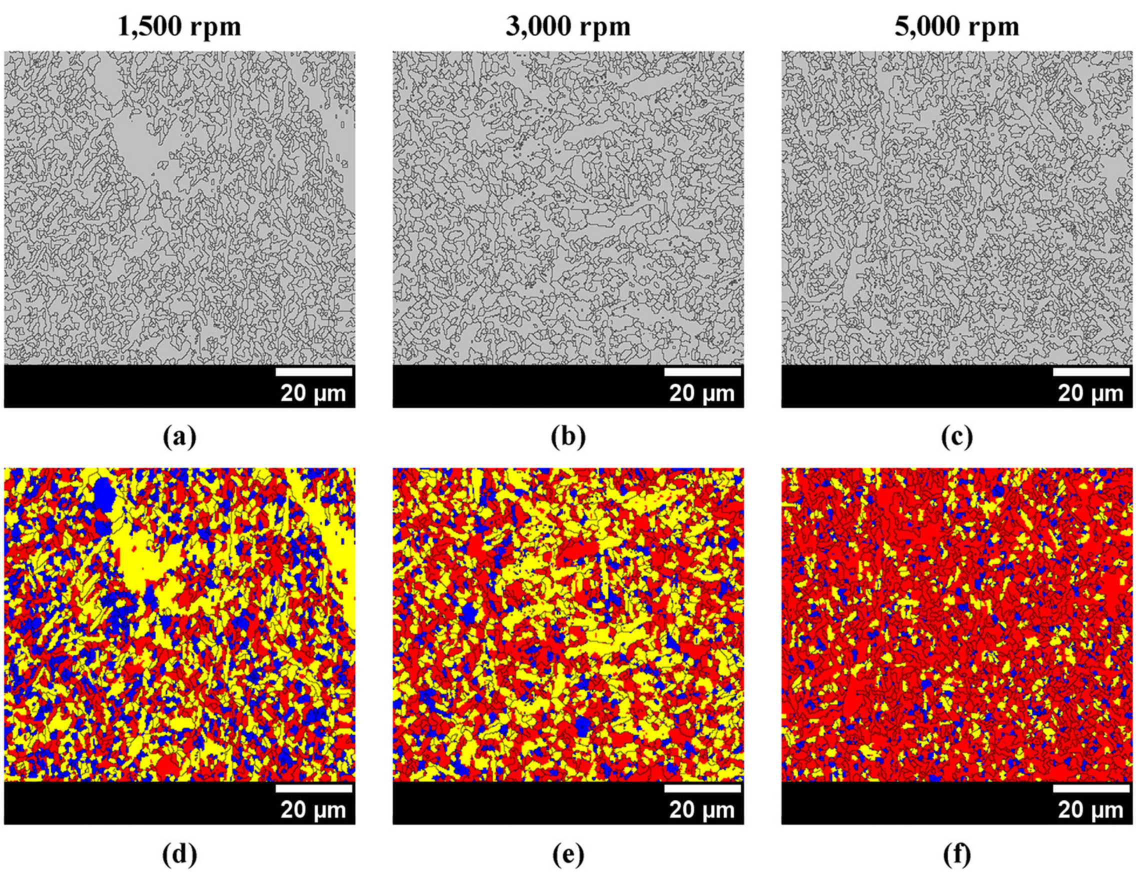

Fig. 10 EBSD results of the BOP samples for 3-mm rotation diameter. Magnification, × 1000. **a**, **b**, **c** Grain orientation map; **d**, **e**, **f** grain average misorientation map

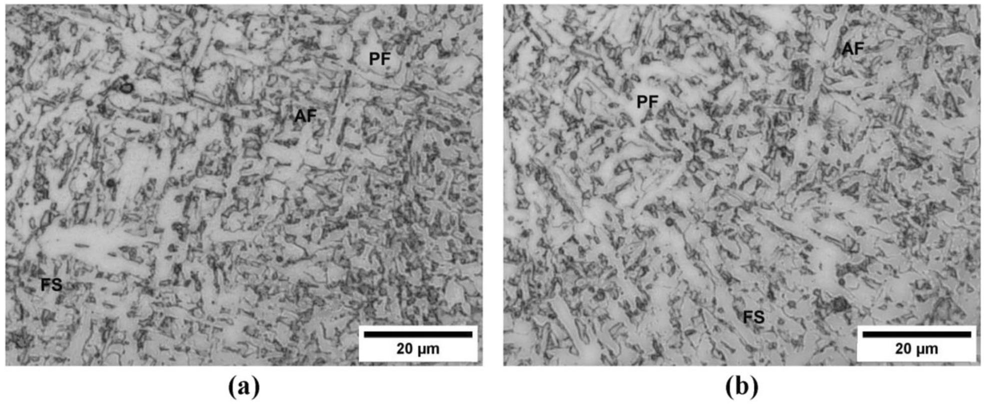

Fig. 12 Microstructure of weld metal after etching with 2% nital (OM). **a** Columnar region and **b** reheated region, where AF, acicular ferrite; FS, ferrite with second phase; PF, primary ferrite

reduction of others alloying elements in comparison with the proposed for "pure" weld metal. As consequence, a detailed metallographic analysis was performed to precisely determinate the presence of the principal parameters contributing to the mechanical properties, such as microstructural constituents, microphases, and inclusions [35].

The metallographic examination revealed a microstructure where the presence of primary ferrite (PF), acicular ferrite (AF), and ferrite with second phase (FS) are observed. These results are in accordance with the available literature for weld metals of the class 700 MPa [16, 38, 42–48]. In addition, the comparison of the columnar and reheated regions (Fig. 12) reveals a homogeneous behavior of the weld metal along thickness. This result also confirmed by the EBSD technique (Figs. 15 and 16) is relevant, because this homogeneity makes the high-strength steel weld metals less dependent on the influence of recrystallization produced by the multiple passes to achieve adequate mechanical properties and does not compromise the higher productivity obtained by the MCAW-RE process. In this work, the proportion of columnar region at the Charpy-V notch was superior to 75%.

Mukhopadhyay et al. [49] stated that proper weld joints can be achieved by a suitable matching of the consumable electrode and the shielding gas mixture. In this respect, Mvola et al. [50] state that the use of a mixture containing 5 to 25% CO_2 is suitable for low alloy steels, because the addition of CO_2 stabilizes the arc, changes the arc characteristic, and results in an increase of the metal transfer frequency. However, there is a relationship between the microstructure of welds and the shielding gas, because an increase in CO_2 contributes to a coarser microstructure with a higher volume fraction of non-metallic inclusions, besides the growth in the burn rate of alloy elements of the base metal, such as silicon and manganese. Some works have reported changes on the mechanical properties due to the decrease of these alloying elements [37, 51–53]. Inclusions formed in the weld metal have two opposing effects on the impact toughness. On one hand, refined inclusions assist the intragranular nucleation of acicular ferrite that refines the weld metal microstructure and improves the toughness. On the other hand, coarser inclusions can initiate brittle cracks or voids during ductile failure [54–56].

In this work, all these factors, dilution, filler metal, and the shielding gas, had influence on the properties of weld metal, due to their effect on the chemical composition and

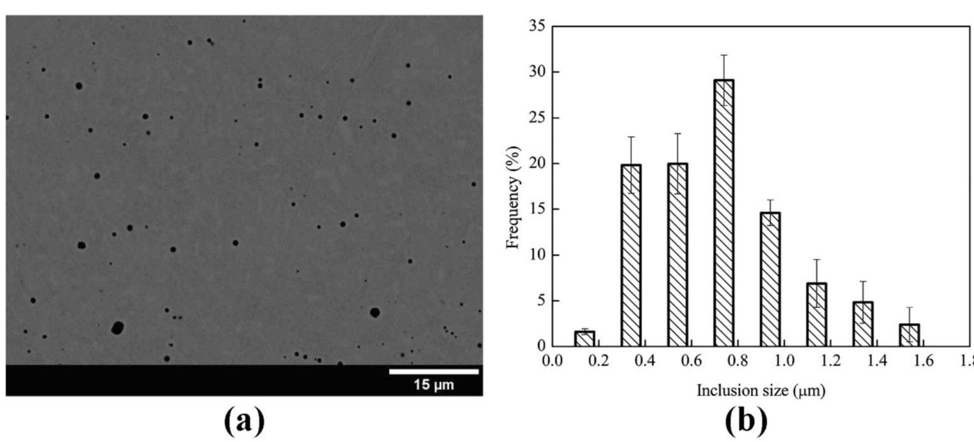

Fig. 13 Inclusions characteristics observed in weld metal. **a** SEM image and **b** Size distribution

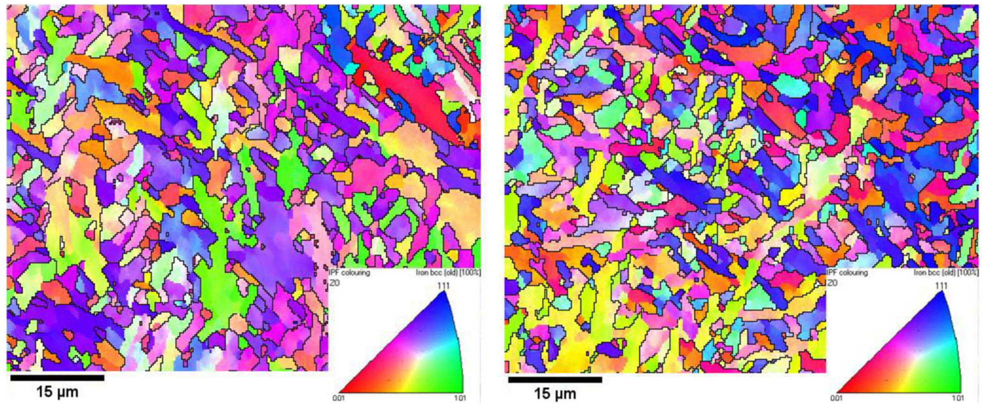

Fig. 15 Image quality maps of the welded joint. **a** Columnar region and **b** reheated region

microstructure. Indeed, while the increase in carbon content as consequence of higher dilution is a contributing factor for obtaining low impact toughness [40, 57], the addition of titanium [35, 57–64] promoted the formation of small inclusions (Fig. 13) and refined the microstructure (Fig. 12). In addition, it is important to mention that both factors contribute to the refined microstructure with higher amount of acicular ferrite than the expected for similar weld metals [44, 46, 48, 65] obtained in this work. Finally, a significant influence of the MA constituents (Fig. 14) on the mechanical properties is not expected, because they are not necklacing the grain boundaries [48, 58, 59, 66].

The microstructural characteristics were responsible for satisfactory mechanical properties, both microhardness (Fig. 17) and impact toughness (Fig. 18), reaching the requirements of several industrial applications.

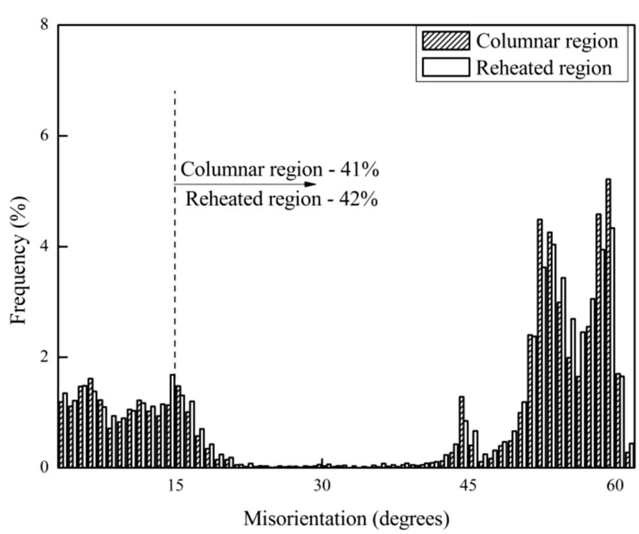

Fig. 16 Misorientation profile of the weld metal

4.3 Practical aspects

First of all, in regard to the costs and productivity, it is important to remember that the conducted experiment in this work was performed with the intention to obtain a welded joint free of defects and, therefore, to test the potential of the process to reach the requirements of some current standards. This goal was achieved using equivalent heat inputs (Table 6), and particularly, the productivity was higher than that obtained by the conventional GMAW process [41], as expected [67].

It is important because the literature registers [68] alternatives as cold wire gas metal arc welding (CW-GMAW), as advantageous process in comparison with rotating electrode process due to its reduced cost and dilution to weld high-strength pipeline steels in narrow gap configuration. However, no records of mechanical properties usually required for qualification of welding procedures are presented, besides some questions related to the lack of penetration due to the arc pinning to the cold wire, which limits the penetration and dilution. On the contrary, their results showed higher hardness values due to the higher cooling rates, which can be an additional problem when welding high-strength steels for pipelines or mooring equipment due to the risk of cold cracking.

As previously mentioned, GMAW-RE process has been studied as a more productive alternative to conventional GMAW process due to the reduction of the deposited weld metal by adopting a square groove (Fig. 1). Table 6 shows a comparison with some characteristics obtained from conventional GMAW process in previous work [41], where advantages of MCAW-RE process is clearly seen. Indeed, it is observed an increase of about 33% in productivity when compared with conventional GMAW process. Consistent results are also observed when comparing GMAW-RE and MCAW-RE welds, because metal cored wire allows a higher

Fig. 14 SEM images showing the microphases occurring in weld metal after etching with 2% nital. **a** Columnar region and (**b**) reheated region

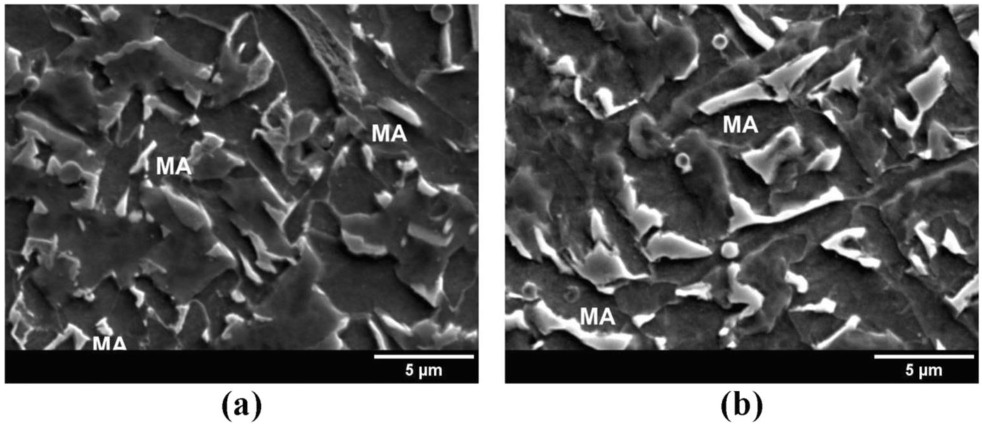

deposition rate than solid wire [67, 69–71]. This advantage has attracted the attention of many researchers in the past two decades [70].

An economic analysis of the welded joints performed in the present work showed that MCAW-RE provided a cost of 21% less than GMAW, despite the higher price of the welding consumable applied (~ 33%), which is in agreement with the literature that reports that metal-cored wires are 30–35% costlier than solid wire [71]. It is an important result because the literature registers [72] that the use of narrow groove is profitable starting from 12-mm thickness.

Although it could be recognized the relevance of the above discussion, it is worth noting that the main goal of this work is to study the mechanical and microstructural properties of the weld metals obtained by these processes, because the available data is limited and needs complementation [23, 24, 41].

Regarding to the mechanical properties, since there are no available data to compare with the results obtained in this work, a comparison with experiments conducted with MCAW process by different authors has been made [38, 44, 73–76]. For this purpose, the Pcm carbon equivalent was adopted to permit a direct comparison with literature data, in order to rationalize the effect of different chemical composition into a single parameter, as suggested by Karlsson et al. [38].

Figure 19 shows the results of impact toughness obtained in the present work in comparison with other investigations involving MCAW welds [38, 44, 73–76]. Corrections were applied for the Charpy-V sub-size specimens (5 × 10 × 55 mm) to compare the results with those of standard samples (10 × 10 × 55 mm) by multiplying the absorbed energies by a factor of 2. It followed many other studies on corrections for sub-sized Charpy-V Notch

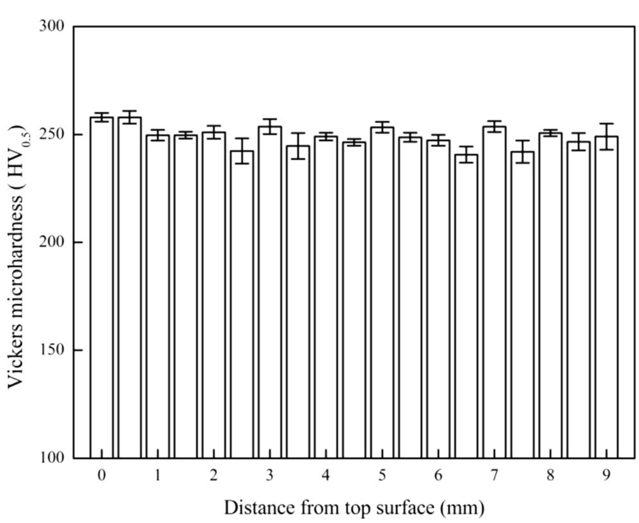

Fig. 17 Results of Vickers microhardness tests

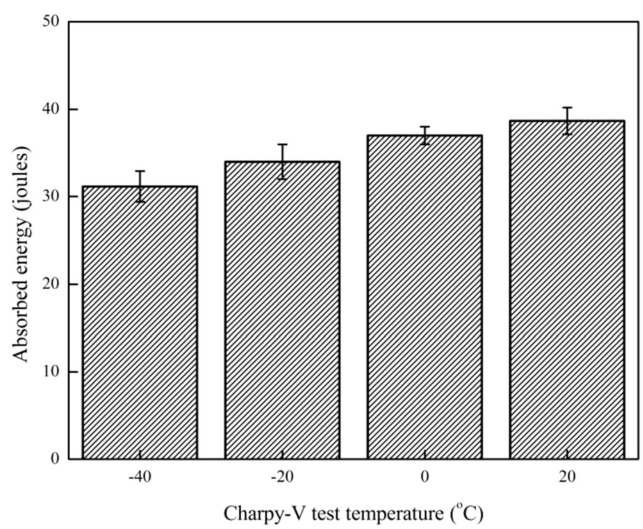

Fig. 18 Results of sub-size Charpy-V impact tests performed at different temperatures

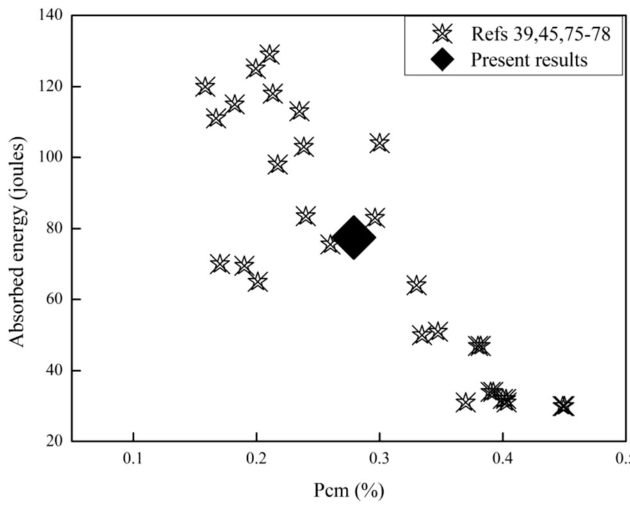

Fig. 19 Relationship between Pcm and impact toughness at 20 °C temperature for weld metals obtained with MCAW process by several works and the present results [38, 44, 73–76]

(CVN) specimens [1, 77–80], where it was postulated that the only correction that was required was for the thickness if the only nonstandard dimension for the test specimens was the thickness. The same procedure is permitted by some standards [80].

From Fig. 19, it is clear that, regardless the less number of passes and higher level of dilution due to the adoption of square groove, the results obtained in the present work are within the same scatter band of the other multi-pass groove butt joints performed by GMAW process using cored wires [38, 44, 73–76]. It can be explained by the radial movement of the arc which promotes a lower peak of temperature in the weld center line [81] and an improvement on the impact toughness [41].

Another crucial information is relative to the achievement of the requirements of several current standards [76, 82–85], making the MCAW-RE process also useful for important industrial applications, such as pipelines, mooring equipment, and ships.

According to Surian [86], although consumables suitable for welding of high-strength steels have been extensively studied, most reports are related to the "pure weld metal." As consequence, the development of specific welding procedure is still required to the appropriate performance of the weld deposits for each base metal. So, the investigation conducted in this work is representative, because the results were similar to those obtained with "pure weld metal," even executing a procedure simulating a real condition.

Based on the above discussed, it is inferred that the GMAW with rotating electrode process using metal-cored wire (MCAW-RE) seems to be an interesting alternative to the conventional GMAW process, due to the higher productivity, lower costs, and adequate mechanical properties.

Table 6 Parameters used for producing the welded joints with 10-mm thickness.

Parameters	GMAW [42]	GMAW-RE [42]	MCAW-RE
Joint geometry	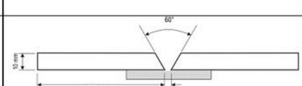	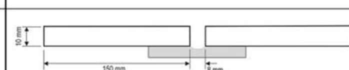	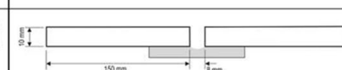
Number of passes	3	2	2
Heat input (kJ/mm)	2.1	2.3	2.0
Length of wire (m)	124.3	90.8(-27%)	93.0(-25%)
Arc time (min)	17.4	11.5(-34%)	10.7(-39%)
Volume of shielding gas (L)	349	230(-34%)	214(-39%)
Volume of deposited weld metal (kg)	1.10	0.81(-27%)	0.83(-25%)
Deposition rate (kg/h)	3.80	4.21(+11%)	4.64(+22%)
Average result		+30%	+33%

5 Conclusions

Based on the results obtained in the present work, the main conclusions are as follows:

1. The rotation frequency and rotation diameter influence the behavior of weld beads. Higher values of rotation frequencies and rotation diameters are not recommended, because they contribute to the existence of welding defects.
2. An association of 1500-rpm and 3-mm diameter is adequate to weld joints with 10-mm thickness.
3. High-strength steel weld metals with adequate mechanical properties can be obtained by MCAW-RE process.
4. The GMAW process with rotating electrode using metal cored wire (MCAW-RE) is an interesting alternative for industrial application, because it promotes a significant improvement on the productivity and the reduction of costs associated with adequate mechanical properties.

Acknowledgments The authors thank the following institutions for the support provided in the execution of the present work: CEFET/RJ, White Martins Gases Industriais Ltda., Centro Tecnológico do Exército (CTEx), CNPq, and FINEP.

References

1. Guo W, Li L, Dong S, Crowther D, Thompson A (2017) Comparison of microstructure and mechanical properties of ultra-narrow gap laser and gas-metal-arc welded S960 high strength steel. Opt Lasers Eng 91:1–15
2. Bunaziv I, Akselsen OM, Frostevarg J, Kaplan AFH (2019) Application of laser-arc hybrid welding of steel for low-temperature service. Int J Adv Manuf Technol. 102:2601–2613. https://doi.org/10.1007/s00170-019-03304-1
3. Berdnikova O, Pozniakov V, Bernatskyi A, Alekseienko T, Sydorets V (2019) Effect of the structure on the mechanical properties and cracking resistance of welded joints of low-alloyed high-strength steels. Proc Struct Integrity 16:89–96
4. Chauhan J (2017) Review paper on gas metal arc welding (GMAW) of mild steel 1018 by using Taguchi technique. Int J Cur Eng Scientific Res 4(7):57–62
5. Devakumaran K, Ananthapadmanaban MR, Ghosh PK (2015) Variation of chemical composition of high strength low alloy steels with different groove sizes in multi-pass conventional and pulsed current gas metal arc weld depositions. Def Technol 11:147–156
6. Saha MK, Das S (2018) Gas metal arc weld cladding and its anti-corrosive performance- a brief review. Athens J Technol Eng 5(2): 155–174
7. Norrish J (2017) Recent gas metal arc welding (GMAW) process developments: the implications related to international fabrication standards. Weld. World 61:755–767
8. Guzman-Flores I, Vargas-Arista B, Gasca-Dominguez J, Cruz-Gonzales CE, Gonzalez-Albarrán MA, Prado-Villasana J (2017) Effect of torch weaving on the microstructure, tensile and impact resistances, and fracture of HAZ and weld bead by robotic GMAW process on ASTM A36 steel. Sold Insp 22(1):72–86
9. Wang JY, Ren YS, Yang F, Guo HE (2007) Novel rotation arc system for narrow gap MAG welding. Sci Technol Weld Join 12(6):505–507
10. Prasad V, Babu M, Ajay P (2018) A review on rotating arc welding process. Mater Today 5:3551–3555
11. Guo N, Han Y, Jia C, Du Y (2011) Effects of wire rotating frequency on metal transfer process in rotating arc narrow gap horizontal GMAW. Adv Mater Res 189-193:3395–3399
12. Kah P, Suoranta R, Martikainen R (2013) Advanced gas metal arc welding processes. Int J Adv Manuf Technol 67(1-4):655–674
13. Li W, Gao K, Wu J, Wang J, Ji Y (2015) Groove sidewall penetration modeling for rotating arc narrow gap MAG welding. Int J Adv Manuf Technol 78:573–581
14. Raju D, Raju G (2016) Effect of using a rotating electrode in GMAW on weld bead characteristic of aluminum alloy 6061-T6 weldment. Proceedings of the World Congress on Engineering 2016, Vol II, London, U.K, July 2016.
15. Santos AGM, Brito HO, Direne HF, Okuyama MP, Schwedersky MB, Silva RHG (n.d.) Soldagem MIG/MAG com eletrodo rotativo destinado a tubulações, Anais da Rio Oil & Gas Expo and Conference 2018, 24-27 setembro, Rio de Janeiro, Brasil, 1-10
16. Zhang T, Li Z, Ma S, Kou S, Jing H (2016) High strength steel (600–900 MPa) deposited metals: microstructure and mechanical properties. Sci Tech Weld Join 21(3):186–193
17. Guo N, Lin SB, Gao C, Fan CL, Yang CL (2009) Study on elimination of interface defects in horizontal joints made by rotating arc narrow gap welding. Sci Technol Weld Join 14(6):584–586
18. Guo N, Wang M, Guo W, Yu J, Feng J (2014) Study on forming mechanism of appearance defect in rotating arc narrow gap horizontal GMAW. Int J. Adv. Manuf Technol 75(1-4):15–20
19. Yang CL, Guo N, Lin SB, Fan CL, Zhang YQ (2009) Application of rotating arc system to horizontal narrow gap welding. Sci Technol Weld Join 14(2):172–177
20. Bai Q, Guo N, Han Y, Zhang J, Wang M (2012) Analysis of temperature distribution in rotating arc welding. Adv Mater Res 472-475:1346–1352
21. Xu G, Li L, Wang J, Zhu J, Li P (2018) Study of weld formation in swing arc narrow gap vertical GMA welding by numerical modeling and experiment. Int J Adv Manufac Technol 96(5-8):1905–1917
22. Shinji I, Masatoshi M, Yuji K (2009) Application of narrow gap welding process with high speed rotating arc to box column joints of heavy thick plates. JFE Tech. Report 14(12):16–21
23. Xu WH, Lin SB, Fan CL, Yang CL (2014) Evaluation on microstructure and mechanical properties of high-strength low-alloy steel joints with oscillating arc narrow gap GMA welding. Int J Adv Manuf Technol 75:1439–1446
24. Venkatesh G, Sundararaj P, Verma DK, Arulkumar J (2018) Comparison of mechanical and metallurgical properties of conventional GMAW with spin arc GMAW process for carbon steel SA 515. Int Res J Eng Technol 5(5):2716–2721
25. American Welding Society. Specification for low alloy steel electrodes, rods for gas shielded arc welding, AWS, 5.28, Miami, FL: AWS; 1996
26. Dias-Fuentes M, Iza-Mendia A, Gutierrez I (2003) Analysis of different acicular ferrite microstructures in low-carbon steels by electron backscattered diffraction. Study of their toughness behavior. Met Mat Trans A 34A:2505–2516
27. Wang Y, Li L (2016) Microstructure evolution of fine-grained heat affected zone in type IV failure of P91 welds. Weld J 95(1):27s–36s
28. Wang Y, Kannan R, Zhang L, Li L (2017) Microstructural analysis of the as-welded heat-affected zone of a grade 91 steel heavy section weldment. Weld J **96**(6):203s–219s

29. Rao, PS, Gupta OP, Murty SSN (2004) A study on the weld bead characteristics in pulsed gas metal arc welding with rotating arc. Proceedings of OMAE04, 23rd International Conference on Offshore Mechanics and Arctic Engineering June 20-25, 2004, Vancouver, British Columbia, Canada, Paper OMAE 2004-51580
30. Kumar S, Rao PS, Ramakrishna A (2011) Effects of eccentricity and arc rotational speed on weld bead geometry in pulsed GMA welding of 5083 aluminum alloy. J Mech Eng Res 3(6):186–196
31. Xu WH, Dong CL, Zhang YP, Yi YY (2017) Characteristics and mechanisms of weld formation during oscillating arc narrow gap vertical up GMA welding. Weld World 61:241–248
32. Guidelines for the classification of ferritic steel weld metal microstructure constituents using the light microscope. IIW DOC. IX-1533-88, 1988.
33. Shrestha SL, Breen AJ, Trimby P, Proust G, Ringer SP, Cairney JM (2014) An automated method of quantifying ferrite microstructures using electron backscatter diffraction (EBSD) data. Ultramicroscopy 137:40–47
34. Gourgues AF, Flower HM, Lindley TC (2000) Electron backscattering diffraction study of acicular ferrite, bainite, and martensite steel microstructures. Mater Sci Tech 16:26–40
35. Jorge JCF, Bott IS, Souza LFG, Mendes MC, Araújo LS, Evans GM (2019) Mechanical and microstructural behavior of C-Mn steel weld deposits with varying titanium contents. J Mater Res Technol 8:4659–4671
36. Duan B, Wang JC, Lu ZH, Zhang GX, Zhang CH (2018) Parameter analysis and optimization of the rotating Arc NG-GMAW welding process. Int J Simul Model 17:170–179
37. Gouda M, Takahashi M, Ikeuchi K (2005) Microstructures of gas metal arc weld metal of 950 MPa class steel. Sci Technol Weld Join 10(3):369–377
38. Karlsson L, Svensson LE, Hurtig K (2014) Influence of dilution on properties of high strength steel weld metals. Biul Inst Spaw 5:62–70
39. Sun YL, Obasi B, Hamelin CJ, Vasileiou AN, Flint TF, Balakrishnan J, Smith MC, Francis JA (2019) Effects of dilution on alloy content and microstructure in multi-pass steel welds. J Mater Proces Tech 265:71–86
40. An T, Wei J, Zhao L, Shan J, Tian Z (2019) Influence of carbon content on microstructure and mechanical properties of 1000 MPa deposited metal by gas metal arc welding. J Iron Steel Res Int 26:512–518
41. Costa JFM, Silva Filho WA, Silveira GMS, Almeida FAC, Lobato MM, Chuvas TC et al (2019) Comportamento de juntas soldadas de aço C-Mn obtidas pelo processo GMAW-RE com eletrodo rotativo. Sold Insp. https://doi.org/10.1590/0104-9224/SI24.11
42. Svensson LE (1999) Consumables for welding high strength steels. Svetsaren 1:30–33
43. Gianetto JA, Bowker JT, Dorling DV, Horsley D (2004) Structure and properties of X80 and X100 pipeline girth welds. Proceedings of IPC2004 International Pipeline Conference, Calgary, Alberta, Canada, 1-13, IPC2004-316
44. Farneze HN, Jorge JCF, Souza LFG, Bott IS (2010) Comparative study of high-strength steel weld metals obtained by the SMAW and FCAW processes for offshore applications and mooring chains. Weld Int 24:903–910
45. Kitagawa Y, Kawasaki H (2013) Recent development of high-strength and tough welding consumables for offshore structures. Kobelco Tech Rev 32(12):1–8
46. Jorge JCF, Souza LFG, Couto JLS, Bott IS (2016) Influence of chemical composition on the mechanical properties of high strength steel weld metals for application in mooring components. Int J Eng Tech Res 4(2):71–76
47. Wang HH, Li GQ, Wan XL, Nune KC, Li Y, Wu KM (2017) Microstructural characteristics and impact toughness in YS690MPa steel weld metal for offshore structures. Sci Technol Weld Join 22(2):133–142
48. Bai F, Ding H, Tong L, Pan L, Wang L (2019) Microstructural changes and impact toughness of fill pass in X80 steel weld metal. Metals. https://doi.org/10.3390/met9080898
49. Mukhopadhyay S, Pal TK (2006) Effect of shielding gas mixture on gas metal arc welding of HSLA steel using solid and flux-cored wires. Int J Adv Manuf Technol 29:262–268
50. Mvola B, Kah P (2017) Effects of shielding gas control: welded joint properties in GMAW process optimization. Int J Adv Manuf Technol 88:2369–2387. https://doi.org/10.1007/s00170-016-8936-2
51. Svoboda H, Rissone N, de Vedia L, Surian E (2004) The effect of welding procedure on ANSI/AWS A5.29-98 E81T1-Ni1 flux cored Arc weld metal deposits. Weld J 83(11):301s–307s
52. Seo JS, Lee C, Kim HJ (2013) Influence of oxygen content on microstructure and inclusion characteristics of bainitic weld metals. ISIJ Int. 53(2):279–285
53. An T, Tian Z, Shan J, Wei J (2015) Effect of shielding gas on microstructure and performance of 1000 MPa grade deposited metals. Acta Metal Sin 51(12):1489–1499
54. Terashima S, Bhadeshia H (2006) Size distribution of oxides and toughness of steel weld metals. Sci Technol Weld Join 11(5):580–582
55. Lan L, Kong X, Qiu C, Zhao D (2016) Influence of microstructural aspects on impact toughness of multi-pass submerged arc welded HSLA steel joints. Mater Des 90:488–498
56. Pamnani R, Jayakumar T, Vasudevan M, Sakthivel T (2016) Investigations on the impact toughness of HSLA steel arc welded joints. J Manufact Proc 21:75–86
57. Jorge et al., (2020) Influence of carbon and manganese on the microstructure evolution of C-Mn-Ti steel weld deposits, IIW DOC.II-A-383-20
58. Wang B, Liu X, Wang G (2018) Inclusion characteristics and acicular ferrite nucleation in Ti-containing weld metals of X80 pipeline steel. Met Mater Trans A. https://doi.org/10.1007/s11661-018-4570-y
59. Han C, Li K, Liu X, Cao R, Cai Z (2018) Effect of Ti content and martensite–austenite constituents on microstructure and mechanical property. Sci Technol Weld Join 23(5):410–419
60. Song FY, Shi MH, Wang P, Zhu FX, Misra RDK (2017) Effect of Mn content on microstructure and mechanical properties of weld metal during high heat input welding processes. J Mater Eng Perform 26(6):2947–2953
61. Seo K, Kim K, Kim H, Ryoo H, Evans GM, Lee C (2019) Microstructural and inclusion characteristics of C–Mn steel welds at a minimal level of titanium. Met Mater Int. https://doi.org/10.1007/s12540-019-00390-4
62. Kang Y, Jang J, Park JH, Lee C (2014) Influence of Ti on non-metallic inclusion formation and acicular ferrite nucleation in high-strength low-alloy steel weld metals. Met Mater Int 20(1):119–127
63. Hu J, Du L, Zhang B, Qi X, Gao X, Misra RDK (2018) Structure–property relationships in heat-affected zone of gas-shielded arc-welded V–N microalloyed steel. J Iron Steel Res Int. https://doi.org/10.1007/s42243-018-0192-2
64. Wen C, Wang Z, Deng X, Wang G, Misra RDK (2018) Effect of heat input on the microstructure and mechanical properties of low alloy ultra-high strength structural steel welded joint. Steel Res Int. https://doi.org/10.1002/srin.201700500
65. Mao G, Cao R, Cayron C, Logé R, Guo X, Jiang Y, Chen J (2018) Microstructural evolution and mechanical property development with nickel addition in low-carbon weld butt joints. J Mater Process Tech. 262:638–649
66. Wang ZQ, Wang XL, Nan YR, Shang CJ, Wang XM, Liu K, Chen B (2018) Effect of Ni content on the microstructure and mechanical

properties of weld metal with both-side submerged arc welding technique. Mater Charact 138:67–77
67. Myrers D (2002) Metal cored wires: advantages and disadvantages. Weld J 81(9):39–42
68. Ribeiro RA, Assunção PDC, Santos EBF, Filho AAC, Braga EM, Gerlich AP (2019) Application of cold wire gas metal Arc welding for narrow gap welding (NGW) of high strength low alloy steel. Materials. https://doi.org/10.3390/ma12030335
69. Garcia RP, Scotti A (2011) A methodology for comparative analyses of the productive capacity between solid (GMAW) and tubular wires (FCAW). Sold Insp 16(2):146–155 (in Portuguese)
70. Lin Z, Goulas ZYW, Hermans MJM (2019) Microstructure and mechanical properties of medium carbon steel deposits obtained via wire and arc additive manufacturing using metal-cored wire. Metals 9(673):1–15
71. Prajapati PJ, Badheka VJ (2019) Investigation on three different weldments on performance of SA516 Gr70 steel material. Alex Eng J 58:637–646
72. Min O, Xin T, Feng L, Shun Y (2011) Welding of quenched and tempered steels with high-spin arc narrow gap MAG system. Int J Adv Manuf Technol 55(5-8):527–533
73. Kang BY, Kim HJ (2000) Effect of Mn and Ni on the variation of the microstructure and mechanical properties of low-carbon weld metal. ISIJ Int 40(12):1237–1245
74. Haslberger P, Ernst W, Schneider C, Holly S, Schnitzer R (2018) Influence of inhomogeneity on several length scales on the local mechanical properties in V-alloyed all-weld metal. Weld World 62(6):1153–1158
75. Schnitzer R, Zügner D, Haslberger P, Ernst W, Kozeschnik E (2017) Influence of alloying elements on the mechanical properties of high-strength weld metal. Sci Technol Weld Join 22(6):1–9
76. Rissone NMR, Svoboda HG, Surian ES, de Vedia LA (2005) Influence of procedure variables on C-Mn-Ni-Mo metal cored wire ferritic all-weld metal. Weld J 84(9):139 s–148 s
77. Chao YJ, Ward JD, Sands RG (2007) Charpy impact energy, fracture toughness and ductile–brittle transition temperature of dual-phase 590 steel. Mater Des 28:551–557
78. Wallin K (2001) Upper shelf energy normalization for sub-sized Charpy-V specimens. Int J Press Vessel Pip 78:463–470
79. Schneider C, Ernst W, Schnitzer R, Staufer H, Vallant R, Enzinger N (2018) Welding of S960MC with undermatching filler material. Weld. World. https://doi.org/10.1007/s40194-018-0570-1
80. American Petroleum Institute (2013) Specification for Line Pipe, API Spec. 5 L, 45th Edition, Washington, USA, July, 192p
81. Guo N, Yanfei H, Zhang L, Zou Y (2011) A modified heat source model for rotating arc welding. China Weld 20(3):58–63
82. International Association of Classification Societies (2011) Offshore Mooring Chain, Specification W22, London: England
83. International Association of Classification Societies, Welding procedure qualification tests of steels for hull construction and marine structures (2012) Specification W28, Rev. 2, London: England
84. Det Norske Veritas, Metallic Materials, Offshore Standard DNV-OS-B101, April 2009, 49p
85. American Bureau of Shipping, Rules for Materials and Welding 2012 (2011) Part 2, Houston, USA, 398p
86. Surian ES (2013) Consumibles para soldadura por arco eléctrico: algunos desarollos recientes. Sold Insp 18(1):77–89